Earth and Planetary Science Letters 584 (2022) 117455

Contents lists available at ScienceDirect

Earth and Planetary Science Letters

www.elsevier.com/locate/epsl

Water enrichment in the mid-ocean ridge by recycling of mantle wedge residue

Jia Liu [a,b], Chunhui Tao [b,c,*], Jianping Zhou [b], Kenji Shimizu [d], Wei Li [b], Jin Liang [b], Shili Liao [b], Takeshi Kuritani [e], Etienne Deloule [f], Takayuki Ushikubo [d], Mitsuhiro Nakagawa [e], Weifang Yang [b], Guoyin Zhang [b], Yunlong Liu [b], Chuanwei Zhu [g], Hao Sun [a], Jingjun Zhou [a]

[a] Key Laboratory of Geoscience Big Data and Deep Resource of Zhejiang Province, School of Earth Sciences, Zhejiang University, Hangzhou 310027, China
[b] Key Laboratory of Submarine Geosciences, Second Institute of Oceanography, Ministry of Natural Resources, Hangzhou, 310012, China
[c] School of Oceanography, Shanghai Jiao Tong University, Shanghai 200240, China
[d] Kochi Institute for Core Sample Research, Japan Agency for Marine-Earth Science Technology (JAMSTEC), Kochi, 783-8502, Japan
[e] Graduate School of Science, Hokkaido University, Sapporo 060-0810, Japan
[f] Centre de Recherches Pétrographiques et Géochimiques, CNRS, Université de Lorraine, Vandoeuvre lès Nancy 54501, France
[g] State Key Laboratory of Ore Deposit Geochemistry, Institute of Geochemistry, Chinese Academy of Sciences, Guiyang 550081, China

ARTICLE INFO

Article history:
Received 21 April 2021
Received in revised form 13 February 2022
Accepted 21 February 2022
Available online 14 March 2022
Editor: R. Hickey-Vargas

Keywords:
MORB
water
H_2O/Ce
mantle wedge
water cycling

ABSTRACT

Trace amounts of water in the sub-oceanic mantle play crucial role in the vigor of mantle convection and the production of oceanic crust, and other many geodynamic processes. Consequently, the cycling of H_2O between the mantle and the exosphere in the mantle is one of the critical processes governing Earth's geodynamical and geochemical evolution. While the deep cycling of altered oceanic lithosphere was considered as the main way to replenish the water in oceanic upper mantle, the significance of the arc mantle wedge after the genesis of arc magmatism dragged down by the subducting slab concomitantly has been not well constrained. Here, we report that fresh depleted basaltic glasses from the ultraslow-spreading Southwestern Indian Ridge (SWIR), located far from any recent subduction zones, show unusually high H_2O/Ce ratios (>600), water contents and heavy hydrogen isotopic compositions. These results could be best explained by recycling of water through melting of a residual hydrous mantle wedge after early melt extraction. Considering that such mantle wedges residue dragged down to the deeper mantle could occupy a volume one order of magnitude larger than that of the subducted lithosphere in the earth history, we suggest that the potential role of such shallow recycling should be considered in studies of global water recycling and the origin of water in the upper asthenosphere.

1. Introduction

Trace amounts of water can affect the rheology and partial melting behavior of the mantle, controlling the vigor of mantle convection and elemental fractionation and transport (Asimow and Langmuir, 2003; Bercovici and Karato, 2003; Hirschmann, 2006; Hirth and Kohlstedt, 2003). The source of normal mid-ocean ridge basalts (MORBs), a widespread layer in the shallow oceanic mantle, is estimated to contain ~50-200 ppm of water (Danyushevsky et al., 2000; Dixon et al., 2017, 2002; Michael, 1995; Saal et al., 2002; Simons et al., 2002). The sub-oceanic ridge mantle tends to be more hydrous when it interacts with an on-, near- or off-axis mantle plume (Asimow and Langmuir, 2003; Bonatti, 1990; Dixon et al., 2002; Gibson and Richards, 2018; Jamtveit et al., 2001), which can transport recycled seawater added to the mantle through deep melting of subducted oceanic lithosphere (igneous crust, sediments or altered lithospheric mantle) (Dixon et al., 2017, 2002; Kendrick et al., 2017), or tap the ancient more-primordial water reservoir in the deep earth (Hallis et al., 2015). The resulting basalts commonly show H_2O contents higher than 0.2 wt.% and "enriched" geochemical signatures, e.g., enhanced fractionation between light and heavy rare earth elements (Asimow and Langmuir, 2003; Dixon et al., 2002; Gibson and Richards, 2018), while their H_2O/Ce ratios vary in a limited range (mostly from ~80 to 350) (Dixon et al., 2002, 2017; Kendrick et al., 2017).

It has long been suggested that the arc-mantle residue in equilibrium with hydrous arc basalts would be depleted in incompatible trace elements and have water contents similar to or higher

* Corresponding author at: Key Laboratory of Submarine Geosciences, Second Institute of Oceanography, Ministry of Natural Resources, Hangzhou, 310012, China.
E-mail address: taochunhuimail@163.com (C. Tao).

https://doi.org/10.1016/j.epsl.2022.117455
0012-821X/

than that in the normal MORB source (Hirschmann, 2006; Hirth and Kohlstedt, 2003). Given that such arc-mantle residue material dragged down to the deeper mantle could constitute a sizable fraction of the mantle in the Earth's history (Hirth and Kohlstedt, 2003), water recycling through recycling of fossil depleted mantle wedge residue would play significant role in the deep water cycling. Based on the major element composition, a few cases have recently indicated that arc mantle segments can exist beneath slow- and ultraslow-spreading ridges (Urann et al., 2020; Gao et al., 2016). Recently, Yang et al. (2021) and Cai et al. (2021) reported that in the ultra-slow spreading Gakkel ridge, some MORB show relatively high H_2O/Ce ratios (up to ~550) and arc-like Nb-Ta depletion. These characteristics have been explained by the recycling of a back-arc-basin-basalt (BABB) mantle.

The Southwestern Indian Ocean Ridge (SWIR) from 46°E to 52°E is located east of the Marion Rise. Within this ocean ridge segment, there is the thickest oceanic crust of the ultraslow-spreading ridges in the world (50.6°E, the Moho depth up to ~10 km below the sea floor (Li et al., 2015)). Close to a harzburgite exposure at 53°E (Zhou and Dick, 2013) (Fig. 1), which was suggested to represent the residue of an ancient arc melt after hydrous partial melting (Gao et al., 2016). Wang et al. (2021) reported the H_2O content of nine glass samples from this ridge, and the resulting H_2O/Ce ratios are all around ~450. In this study, we conducted a comprehensive geochemical study of 50 fresh basaltic glass chips from SWIR 48-52°E and 55°E (Fig. 1), measuring their volatile contents (H_2O, CO_2, Cl, and F), hydrogen, Sr-, and Nd-isotopic compositions. After hydrogen isotopic analysis, the same samples were conducted in-situ boron concentration and $\delta^{11}B$ analysis. In contrast to the previously reported water-enriched melting regimes in oceanic ridges, our results show that the H_2O/Ce ratios of noncontaminated glasses from 48-52°E can be higher than 600, being clearly higher than the values of several presently established mantle end-member (like EM1, EM2, HIMU) (Asimow and Langmuir, 2003; Dixon et al., 2017, 2002; Gibson and Richards, 2018). Coupled with low Ce/Pb ratios, high δD values and depleted $(La/Sm)_N$, these high H_2O/Ce signatures are attributed to a component like the arc-mantle residue after melt extraction. Our modeling calculation shows that such recycling of mantle wedge residue can also transport significant amounts of water into the sub-ocean mantle, not necessarily leading to typical arc-like trace elemental patterns (e.g. Nb and Ta depletion). This would extend our understanding of the global water recycling between the Earth's surface and interior.

2. Materials and methods

Fifty fresh quenched glass chips (see sample description in Supplementary materials and Supplementary Fig. 1) were carefully selected and analyzed for major and trace elements, and H_2O contents. A subset of these samples were analyzed for Cl, F, B and Sr-Nd-H-B isotopes.

2.1. EPMA

Major element compositions of minerals were determined on a JEOL JXA-8100 electron microprobe (EMP) at Key Laboratory of Submarine Geosciences, Second Institute of Oceanography. The working conditions were 15 kV accelerating voltage, 20 nA beam current and 5 μm beam diameter. Natural minerals and synthetic oxides were used as standards and a program based on the ZAF procedure was used for data correction. The analytical error for all elements is below 5%. All EMP analyses were conducted using back-scattered electron (BSE) images for microstructure guidance.

2.2. Trace element analysis by LA-ICP-MS

Trace element compositions of minerals were measured in situ by laser ablation inductively coupled plasma mass spectrometry (LA-ICP-MS) at the Key Laboratory of Crust-Mantle Interaction and Evolution of CAS, University of Science and Technology of China. The laser beam had a diameter of 50 μm, a frequency of 8 Hz and an energy density of 14 J/cm^2. The off-line selection, integration of background and analytical signals, time-drift correction and quantitative calibration for trace elements analyses of minerals were performed using ICPMSDataCal (Liu et al., 2008). Trace element concentrations were calibrated using external standards BCR-2G, BHVO-2G and BIR-1G without internal standards (Liu et al., 2008). The preferred values of element concentrations for the USGS reference glasses were from the GeoReM database (http://georem.mpch-mainz.gwdg.de). The analytical errors for most trace elements are within 10% (2SD). Part of the glasses were analyzed in the LA-ICP-MS lab in School of Earth Sciences, Zhejiang University. The results from these two laboratories are consistent with each other.

2.3. Volatile analysis by FTIR and SIMS

The CO_2 and H_2O contents of the glasses were analyzed by FTIR equipped in School of Earth Sciences, Zhejiang University. Samples were prepared for FTIR analysis by making double-polished thin sections with thicknesses of ~0.05~0.07 mm. Infrared unpolarized spectra were obtained from wavenumber 2500 to 4000 cm^{-1} on a Nicolet FTIR spectrometer IS50 coupled with a Continu μm microscope, using a KBr beam-splitter and a liquid-nitrogen cooled MCT-A detector. A total of 128 scans were accumulated for each spectrum at a 4 cm^{-1} resolution. The aperture size varied from 30×30 μm to 50×50 μm. The thickness of the glass wafer was measured by a digital micrometer with a precision of ±1 μm. The total water content of the glass was calculated by the Beer-Lambert law calibration. The molar absorptivity for total dissolved water using the fundamental OH stretching band at 3535 cm^{-1} is not strongly compositionally dependent on basaltic compositions, and here the value of 63±5 l/mol cm was used (Dixon et al., 1995). The molar absorptivity for carbonate bands (1525 cm^{-1} and 1430 cm^{-1}) is 330±20 l/mol cm (Dixon et al., 1995). An example for the baseline correction is shown in Supplementary materials.

The SIMS analysis for H_2O, CO_2, Cl and F was conducted with a Cameca IMS-1280HR instrument at Kochi Institute for Core Sample Research, Japan Agency for Marine-Earth Science and Technology, Japan. The procedure reported by Shimizu et al. (2017) was followed. The fresh glass separates were mounted on indium and polished well. A 20 keV (10 keV at the ion source and 10 keV at the sample surface) Cs^+ ion beam of 300–500 pA was defocused to be 10–15 mm in diameter. Secondary ions were accelerated at 10 kV, and the transfer optics were set at 200x magnification. A –10 keV electron gun ~100 mm in diameter was applied for electrostatic charge compensation of the analysis area. Only the secondary ion signals from the center of the analysis spot, ~10–15 mm in diameter, were collected in order to eliminate secondary ion signals from surface contamination and the edge of the primary beam. A mass resolving power of ~6000 was applied. Each analysis consisted of 20 s for pre-sputtering, 120 s for auto-centering of secondary ions to the field aperture (X- and Y-directions) and the contrast aperture (X-direction), and 10 cycles for measurements. Multiple natural and synthetic glass standards were used to calibrate the instrumental mass fractionation, and glass standards E-LA, EPRG3 and HWG1 were mounted with the sample together to calibrate the instrumental drift.

The analyses for hydrogen isotopes were conducted with the same SIMS nearby each analytical spot, following the method of

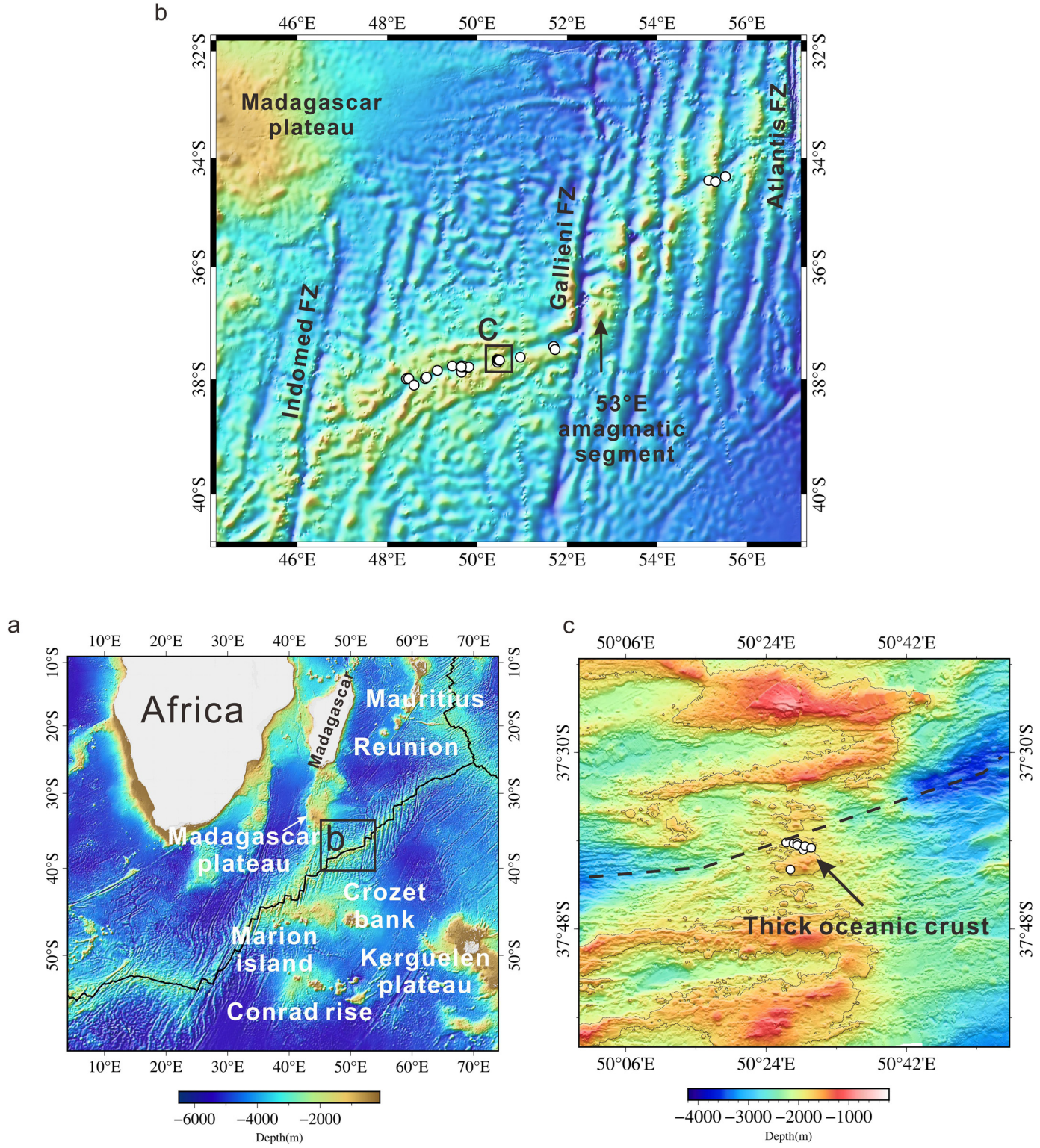

Fig. 1. Sample locations. a, Map showing the location of the Southwestern Indian Ocean Ridge (SWIR). **b**, Map of the studied SWIR segment corresponding to the square in **a**. FZ means transform fault zone. **c**, Water depth map for the region 50.6°E where the oceanic crust thickness can be up to 9.5 km. The white circles indicate the sampling locations and the dashed black line shows the position of the ridge. All maps are made by the GMT software. (For interpretation of the colors in the figure(s), the reader is referred to the web version of this article.)

Shimizu et al. (2019). For hydrogen isotopes, we used a large defocused beam (∼5 nA; ∼15 mm diameter) to decrease the hydrogen background. For analyses of D/H ratios, ^{16}OH and ^{16}OD were measured in multi-detection mode with a Faraday cup and an axial electron multiplier (EM), respectively. Each measurement time was 6–7 min. For hydrogen isotopes, a mass resolving powers of axial EM and FC were set at ∼ 10000 and ∼5000 to sufficiently separate ^{16}OD from ^{18}O, ^{17}OH and ^{16}OHH, and ^{16}OH from ^{17}O, respectively. To determine hydrogen isotope compositions, we applied the standard bracketing method. A working standard glass (HW-G1) for hydrogen isotopes was analyzed 5 times for every 10 unknown samples. By averaging 8–10 data points of the working

standard, the OD/OH IMF and analytical error of 2 SD were calculated. If the 2 SE of the unknown sample was greater than 2 SD, we adopted the former as the analytical error; otherwise, we adopted the latter as the analytical error.

2.4. Boron content and isotopic composition

The boron content and isotopic composition ($\delta^{11}B$) of the sample sets conducted for H isotope were analyzed with Cameca IMS 1270 in CNRS-CRPG, Nancy, France, followed the approach by Bouvier et al. (2008). The B content and $\delta^{11}B$ were measured with a primary O^- beam with intensity of 10 nA. The beam size is 10 μm with accelerate voltage of 10 kv, mass resolution of 2000 and no energy filtering mode. B content was normalized to ^{16}O counts rate, and calibrated based on the B/O measured ratio Gor132Gs (Supplementary Fig. 2). 32 cycles were cumulated on each point, and 5 analysis points were conducted for each sample. The instrumental boron isotopic fractionation was determined by analyzing standards with basaltic compositions (Gor128G, Gor132G). The stand error (SD) of the single point for Gor128G with B of 23.5 ppm is ±1.1‰ to ±1.6‰, while for our samples this typical stand error could be around ±3∼ 4‰. The typical stand error of the five measurements for the samples is from 1.1 to 5.6‰.

2.5. Sr-Nd isotopes analysis

Strontium and neodymium isotope analyses were conducted at the Faculty of Science, Hokkaido University. Powdered samples were leached with 6 M HCl at 80 °C for 1 h to eliminate the effects of seawater alteration. Chemical separation of Sr was performed using Sr-spec resin with an HNO3 medium following the method of Pin et al. (1994). Neodymium was separated using TRU and Ln resins with an HNO_3 and an HCl medium, respectively, following the methods of Pin et al. (1994) and Pin and Zalduegui (1997). Isotopic ratios were determined using a multiple collector (MC)–ICP–MS instrument (Neptune plus, Thermo Fisher Scientific). Mass fractionation factors for Sr and Nd were internally corrected using $^{86}Sr/^{88}Sr = 0.1194$ and $^{146}Nd/^{144}Nd = 0.7219$, respectively. Additional corrections were performed by applying a standard bracketing method using NIST987 and JNdi-1 for Sr and Nd, respectively, and normalizing to $^{87}Sr/^{86}Sr = 0.710240$ for NIST 987 and $^{143}Nd/^{144}Nd = 0.512117$ for JNdi-1.

3. Results

All the glasses have MgO contents >7.0 wt.%, with some of them showing MgO greater than 8.0 wt.% (Supplementary Table 1, Supplementary Fig. 3), which indicates that the extent of fractionation of mafic minerals was not significant. The K_2O contents are generally lower than 0.15 wt.%, except three samples with K_2O from 0.20 to 0.35 wt.% (Supplementary Table 1). All the samples are depleted in light rare earth elements (LREE), with $(La/Sm)_N$ varying from 0.24 to 0.74 and $(Sm/Yb)_N$ varying from 0.65 to 1.41 (Fig. 2). Several samples from 50.6°E have relatively high Al_2O_3 contents, lower HREE contents than $^{143}Nd/^{144}Nd$ (<0.51305) ratios than other samples (Fig. 2, Supplementary Fig. 2), which are consistent with the identification of a high-Al group by Yang et al. (2017). In the following text, we refer to these samples as the high-Al group and other samples from 48°E to 52°E as the main group.

The water contents measured by FTIR vary from 0.06 to 0.57 wt.% (Figs. 3, 4, Supplementary Table 1). The water contents corrected to MgO of 8.0 wt.% ($H_2O_{(8)}$) for the samples from 48°E to 52°E are in the range of 0.06 to 0.58 wt.% (Fig. 3, 4), most of which are higher than the typical values of global MORB (<0.2 wt.%,

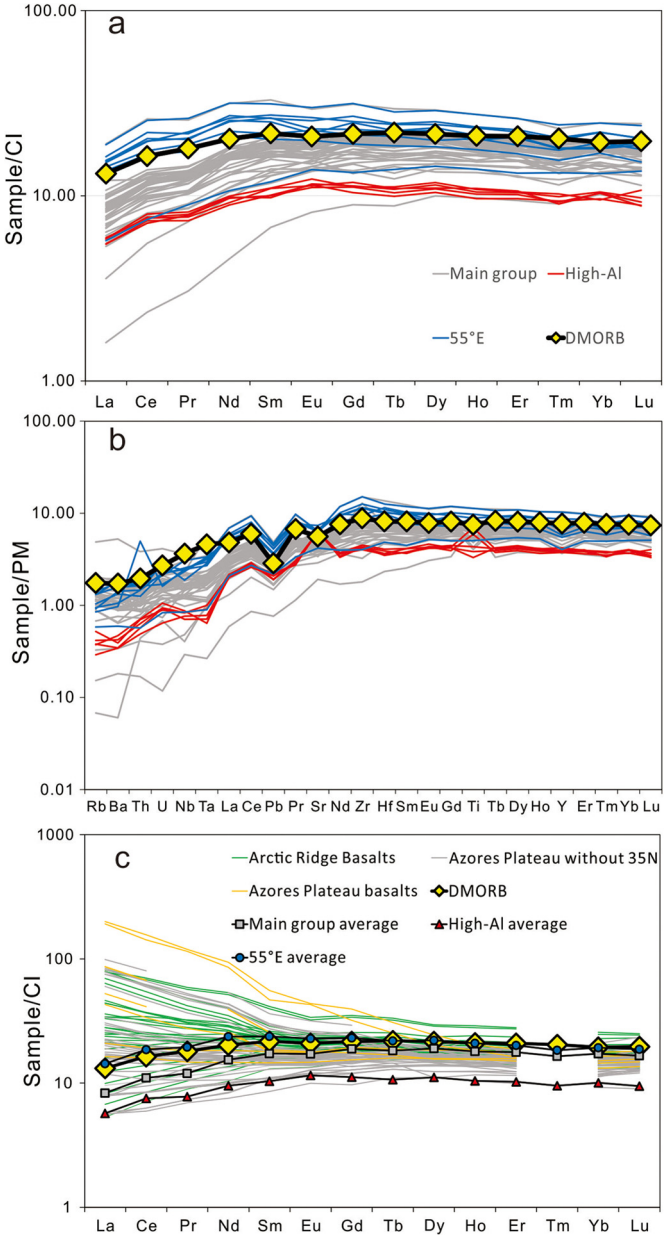

Fig. 2. The chondrite and primitive mantle normalized elemental patterns for the SWIR glasses in this study. **a**, CI-chondrite normalized rare earth elemental pattern. The main group includes the samples from 48°E to 52°E, except the high-Al group samples. D-MORB data is from Gale et al. (2013). The normalization value of CI-chondrite is from Sun and McDonough (1989). **b**, primitive mantle normalized trace elemental pattern. The primitive mantle elemental concentration data is from McDonough and Sun, 1995. **c**, the CI-chondrite normalized rare earth elemental pattern for the glasses from Arctic and north Atlantic ridges. The data are from Dixon et al. (2017) and its supplementary data, see Supplementary Table 7 for data sources. The averages of high-Al, main group and 55°E samples in this study are also shown for comparison.

Danyushevsky et al., 2000). A sub-set of the samples was then analyzed by secondary ion mass spectrometry (SIMS) for H_2O, CO_2, F and Cl concentration and hydrogen isotopic compositions (Supplementary Table 2). These two techniques give rather consistent results for the sample with extreme low water content (0.06 wt.%, 30II-TVG04) and two high-Al samples, while the results for other samples except 34II-TVG12 are comparable around 20% deviation (Supplementary Table 1, 2). Both techniques also result in comparable H_2O/Ce ratios for all samples with SIMS data (Supplementary Fig. 4).

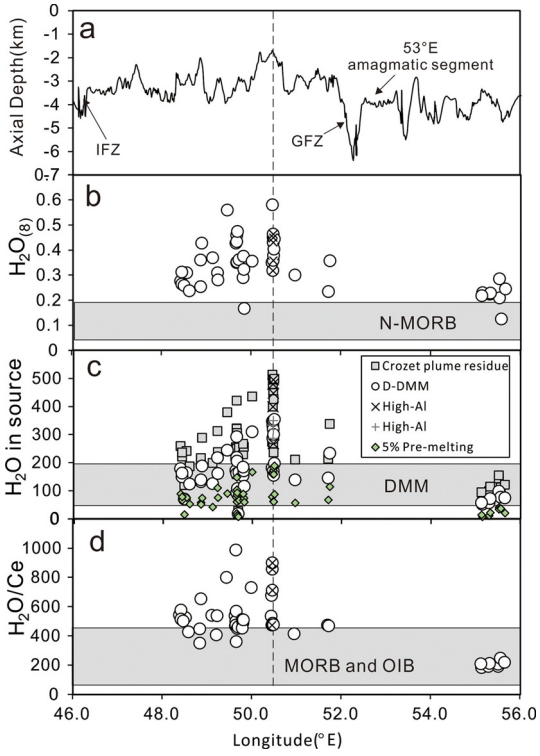

Fig. 3. Variations in the axial depth, H_2O, H_2O/Ce and mantle potential temperature along the SWIR. a, Axial depth of the studied SWIR segments. Data acquired by the Chinese R/V Dayang Yihao. IFZ and GFZ represent Imdomed Transform Fault Zone and Gallieni Transform Fault Zone, respectively. The 53°E amagmatic segment is the location where harzburgites are exposed directly at the ridge. **b**, variation of the water content corrected to MgO of 8.0 wt.%. **c**, variation in the calculated water contents in the mantle source along the oceanic ridge (see Supplementary materials for calculation details). 5% pre-melting refers to the calculation with assumption that the source is the residue of the average-DMM after 5% partial melting. **d**, variation in H_2O/Ce along the oceanic ridge. The gray boxes show the corresponding ranges for MORB or OIB (Hirschmann, 2006).

For the samples from 48°E to 52°E, the high-Al group shows H_2O/Ce ratios from 472 to 1109, while the main group has H_2O/Ce ratios that are mostly higher than 450 and reach up to ~986 (significantly higher than the results of Wang et al. (2021)), being considerably higher than those of global MORB glasses (all <430, mostly <250) (Danyushevsky et al., 2000; Dixon et al., 2017, 2002; Gibson and Richards, 2018) and falling in the range of H_2O/Ce found in arc and back-arc lavas (350-10000) (Cooper et al., 2012) (Fig. 4, 5). The samples from 50.6°E with the supper thick oceanic crust and from 49.6 to 49.8 °E with multiple detachment faults show similarly high H_2O content and H_2O/Ce ratio (Fig. 3). To the contrast, the samples from the 55°E show a limited range in H_2O/Ce from 183 to 245 (Fig. 3, 4). In the whole dataset, the Cl contents vary from 6.6 ppm to 126.8 ppm, with most being lower than 80 ppm. The F contents vary from 43.3 to 238.9 ppm, being mostly less than 150 ppm. The Cl/K ratios fall in the range of 0.01 to 0.15 and are negatively correlated with H_2O/Ce (Fig. 4). The B contents of the measured samples vary from 0.7 to 1.9 ppm, which are in the range of the fresh MORB glasses with Cl/K <0.08 (Marschall et al., 2017) and positively correlated with F and Nb contents (Fig. 6).

The hydrogen isotopic compositions (δD relative to V-SMOW) of the glasses vary from -50±13‰ to -83±13‰ (Supplementary Table 3), and are negatively correlated with F, heavy rare earth elements, such as Y, and Ce/Pb ratio (Supplementary Fig. 5). The $\delta^{11}B$ varies from -10.0±2.0‰ to -1.8±4.5‰ (Supplementary Table 4), which are in the range of global MORB with low Cl/K (<0.08) recently reported by Marschall et al. (2017) (Fig. 7), and some samples with $H_2O/Ce>500$ have $\delta^{11}B$ in the range of the pristine normal MORB (lower than -6.5‰). The 55°E samples, with H_2O/Ce ratios around 200, show $\delta^{11}B$ from –9.5±4.3‰ to -4.1±4.1‰ (average value of -6.9±2.7‰), while their B concentrations span a narrow range from 1.4 to 1.6 ppm. For the 49.6 to 49.8 °E segment, the samples with lower B contents show heavier $\delta^{11}B$ (Fig. 7). In addition, no clear correlations between $\delta^{11}B$ and H_2O/Ce could be identified (Fig. 7). The measured $^{87}Sr/^{86}Sr$ and $^{143}Nd/^{144}Nd$ ratios for the high-Al group samples are from 0.70310 to 0.70340 and from 0.51300 to 0.5130, respectively (Supplementary Table 5).

4. Discussion

4.1. High H_2O/Ce ratios and water contents of the mantle source

Seawater contamination by assimilation of altered oceanic lithosphere and/or hydrothermal brines can potentially overprint the pristine water contents of oceanic glasses. Yang et al. (2017) suggested the primary magma of the high-Al group samples experienced assimilation with the troctolite accumulates in the lower oceanic crust. This melt-rock interactions would provide the chance to elevate the water contents of the final erupted magmas, if those accumulates were extensively hydrated. However, the following observations show that most of the high H_2O/Ce ratios of our samples cannot be attributed to these secondary processes.

The fluid-mobile elements (e.g. Rb, Ba, U, Pb), which are usually enriched in the altered oceanic crust or serpentinized abyssal peridotite to variously extents (Boschi et al., 2013), are well correlated with the fluid-immobile element Nb (Supplementary Fig. 6). Note that our samples are distributed along the ridge segments as long as several hundreds of kilometers, including the segments controlled by both magmatic and tectonic activities (thick oceanic crust vs. mantle directly exposed, Fig. 1) respectively. The assimilation of those different hydrated components in the altered oceanic lithosphere with different backgrounds would lead to random deviation of these elements to different extents, which are not observed. As illustrated in Fig. 4a, most of the measured water contents are positively correlated with K_2O, except for a few samples (e.g., 40I-TVG09, 30III-TVG20-1, and 30IV-TVG04) with relatively high K_2O. The slope for the 55°E samples is like that of the Arctic and north Atlantic ridge basalts, while it is considerably shallower than the slope of the main group and high-Al samples. Similar correlation between H_2O and Ce is also seen for the main group samples, while the water contents of the high-Al group samples vary from 0.23 to 0.50 wt.% at a small range of Ce (Fig. 4b). The samples standing out of the correlations in Fig. 4a,b might have been affected by assimilation of altered and K_2O-rich oceanic crust or sediment. However, as shown in Fig. 4d, even if those high K_2O samples are not considered, the K/Cl ratios of the majority are similar to those of MORB and OIB that are free of contamination, and their scattered trend with H_2O/Cl ratios could not be explained by assimilation of seawater, brines or serpentinized peridotite. The Cl/K ratios of the samples with H_2O/Ce from ~200 to 1109 are all within or below the range of pristine basaltic glasses in slow- or ultraslow-spreading Atlantic and Arctic ridges, which have similar distributions of fracture zones along ridge.

The low Cl/K ratios of some samples were possibly caused by the assimilation of high K_2O hydrous components in the altered lithosphere. The B concentrations and $\delta^{11}B$ give further constraints to this issue. The positive and linear trends between B and F and Nb (Fig. 6) are hard to reconcile with the assimilation of serpentinized peridotite, which has rather high B content (usually >50 ppm) but low Nb (mostly <0.3 ppm) (Boschi et al., 2013) and the assimilation would lead to extensively elevation of B but no significant change of the latter. Although the uncertainty of B isotopic data in this study is large, assimilation of altered oceanic and/or

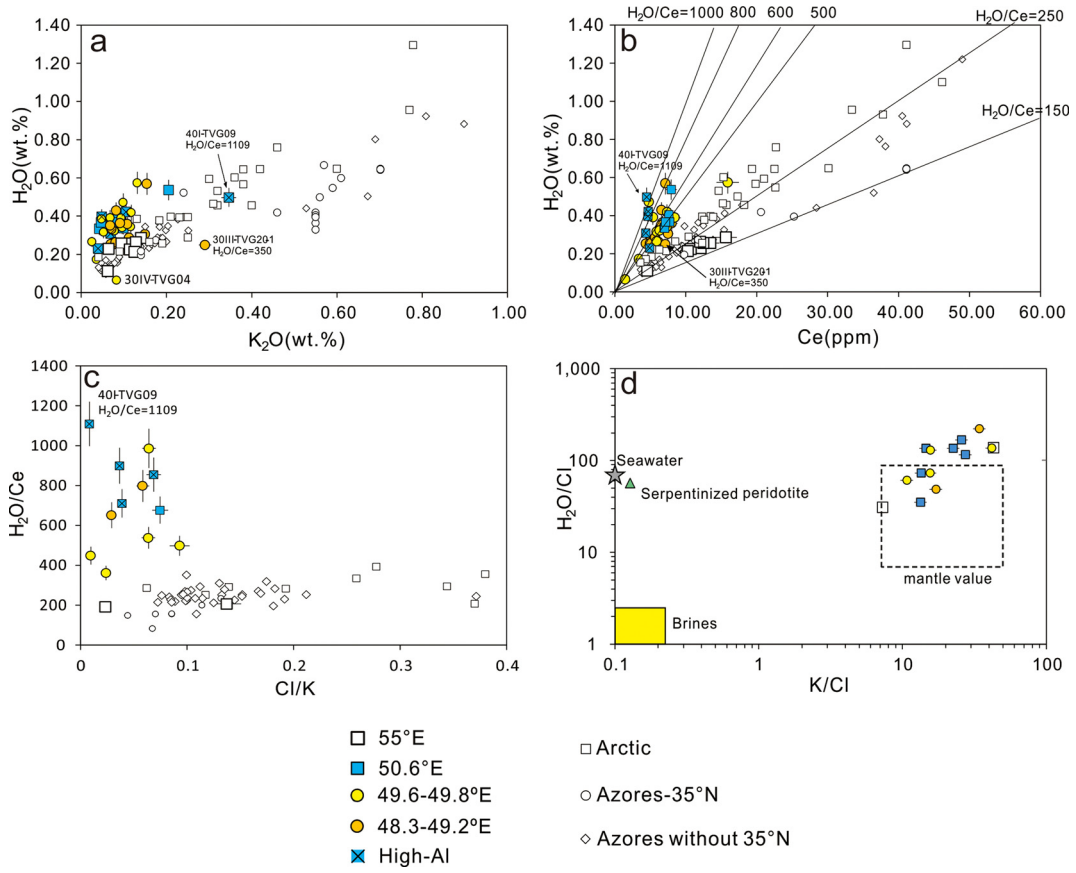

Fig. 4. Comparison of the water contents with other trace element and volatile concentrations in glasses in this study. **a**, H_2O vs. K_2O plot. The horizontal and vertical uncertainties are ±5% and ±10%, respectively. **b**, H_2O vs. Ce plot. The error bars are the same as in **a**. **c**, H_2O/Ce vs. Cl/K plot. **d**, Comparison of H_2O/Cl with K/Cl. The dashed box labeled as "mantle value" represents the ratios in mantle-derived basalts free of seawater assimilation. The data for the mantle, seawater and brines (with brine salinities higher than 50% salts) are from Kendrick et al. (2017) and the data for serpentinized peridotite from Boschi et al. (2013). In **a**, **b** and **c**, compositions of basalt glasses from the Arctic ridge (Mohns, Jan Mayer and Kolbein) and Mid-Atlantic ridge (33°N~40°N, FAZAR cruise) are also plotted for comparison, the data are from the Dixon et al. (2017) and its supporting supplementary dataset. See Supplementary Table 7 for data sources.

serpentinized peridotite cannot explain the data (Fig. 7). For example, assimilation of altered oceanic crust at high-temperature (H-AOC) to 30% mass fraction could only result in slight elevation in $\delta^{11}B$. The assimilation of low-temperature altered oceanic crust (L-AOC) seems difficult to fit the trend in $\delta^{11}B$ vs. B space. The modeling also shows that very small proportion of assimilation of serpentine (1.2 wt.%) could result in the observed high $\delta^{11}B$, but it could not enhance the H_2O/Ce ratio to ~1000.

High H_2O/Ce ratios in olivine-hosted melt inclusions in MORB are not unusual; however, they have been explained by inward-diffusion of water to Ce-depleted melt inclusions (Hartley et al., 2015; Le Voyer et al., 2014). Our fresh quenched glasses would be free of this problem. Finally, the water diffusion coefficient of Zhang and Stolper (1991) at the seawater temperature of 2 °C gives a calculated effective diffusion distance of only 70 μm, even if the assumed diffusion time is 100 Ma, which is much longer than the eruption age of the on-axis basalts (<10 Ma). This means that water could not be enriched by post-eruption diffusion. Although explaining the samples standing out in Figs. 4a and 4b may not be straightforward, we suggest that the sample assimilation of hydrous oceanic crust or peridotite is not easy to reconcile with multiple indexes together (H_2O/Cl, B content and $\delta^{11}B$). However, at least most of the H_2O/Ce ratios of the main group samples from 48 to 52°E, falling in the range of 800 to 600, are not overprinted by contamination but represent their mantle source compositions.

4.2. The water contents of the mantle sources

Following the method of Kelley et al. (2006), we calculated $H_2O_{(90)}$ as the H_2O content normalized to the primary melt in equilibrium with the mantle source. The water contents of the mantle source were then calculated based on these corrected H_2O values and the degrees of partial melting recovered by the partitioning behavior of TiO_2 (Kelley et al., 2006) (see Supplementary materials and Supplementary Table 6). Considering that the mantle sources of the studied ridge may have been experienced previous melting event (Yang et al., 2017; Yu and Dick, 2020), in our calculations we compared the results from several different calculating approaches: (1) the mantle sources are the residue of the Crozet mantle plume; (2) mantle sources after 5% early partial melting of the average DMM of Workman and Hart (2005); (3) mantle sources with TiO_2 of 0.108 wt.% and 0.120 wt.%, which are the depleted- and average- DMM of Workman and Hart (2005). See Supplementary text and data to see the detail of calculations.

The calculated mantle source water contents are shown in Fig. 3. For case (1), the estimated TiO_2 content of the Crozet plume residue after melt extraction is about 0.139 wt.%, rather similar with the TiO_2 content of the DMM defined by Salters and Stracke (2004), which results in the calculated water content of the mantle source varying from ~100 to 510 ppm (Fig. 3). Most of these values are higher than the water contents of MORB sources far from hotspots (50~200 ppm), even if the high-Al samples in Figs. 4a and 4b are not considered. For case (2), the recovered water contents are all <200 ppm. However, the partial melting degrees are

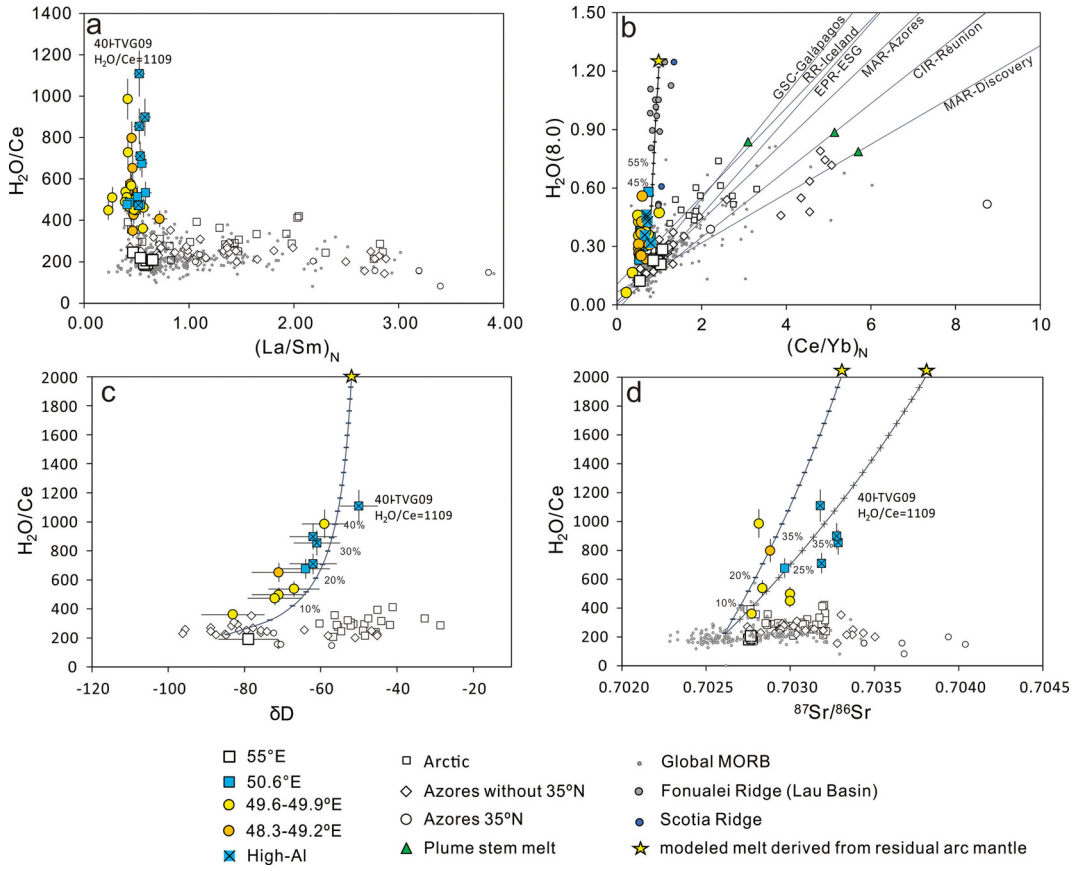

Fig. 5. Water, Sr isotope and trace element systematics of SWIR samples. **a**, H_2O/Ce vs. $(La/Sm)_N$ plot. Artic and FAZAR Mid-Atlantic ridge basalts are the same as in Fig. 2, and data from Dixon et al. (2017). Data for other mid-ocean basalts from ridges are also plotted for comparison (data from PetDB, http://www.petdb.org/), see Supplementary Table 7 for the original data sources. **b**, $H_2O_{(8.0)}/Ce$ vs. $(Ce/Yb)_N$ plot. The black real lines indicate trends for the mid-ocean ridge basalts that have been affected by an on- or near-axis mantle plume through ridge-ward channelized hydrous low-degree melts (Gibson and Richards, 2018). The green real triangles show the modeled mean composition of the plume-derived low-degree melts (Gibson and Richards, 2018). The notes near the lines show pairs of mid-ocean ridges and on- or near-axis plumes. GSC is Galapágos Spreading Centre, RR is Reykjanes Ridge, EPR is East Pacific Rise, ESG is Eastern-Salas y Gomez, MAR is Mid-Atlantic Ridge, and CIR is Central Indian Ridge. Back-arc ridge basalts from Fonualei Ridge and Scotia Ridge are also plotted for comparison, see Supplementary Table 7 for data sources. The curved lines represent mixing between depleted MORB mantle (Workman and Hart, 2005) and modeled partial melts derived from residual arc mantle (see Supplementary material for the modeling calculation). Every step is 5% of the residual arc mantle melt. **c**, H_2O/Ce vs δD plot. **d**, H_2O/Ce vs. $^{87}Sr/^{86}Sr$ plot. Two curved lines show mixing between DMM-derived melts and modeled partial melts of the residual arc mantle, with different initial $^{87}Sr/^{86}Sr$ ratios (see Supplementary Table 7).

generally lower than 2%, with many of the lower than 1%, and event lower than 0.2%. Such low extents of melting would be hard to extract from the mantle source. For case (3), the water contents in 50.6°E could be up to ~350 and ~410 ppm, when the mantle source is assumed to be the depleted- and average-DMM respectively. For all cases, the samples from the thick oceanic crust (50.6°E) always have higher water contents than others. Following, we will discuss the possible reasons for this water enrichment in the mantle sources.

4.3. Water enrichment associated with residuum arc mantle

Mapping of $H_2O_{(8)}$ in basalts from global mid-ocean ridges has revealed that H_2O-rich MORBs tend to occur where the ridge has been interacted with mantle plume (Asimow and Langmuir, 2003; Dixon et al., 2017, 2002; Gibson and Richards, 2018). Although the mechanisms for this water enrichment, either directly by solid flow of a plume mantle or mixing with hydrous low-degree partial melts derived from the plume mantle through channelized melt flow (Asimow and Langmuir, 2003; Dixon et al., 2017, 2002; Gibson and Richards, 2018) remain debatable, the striking observation is that H_2O-rich MORBs usually show "enriched" geochemical signatures to a different extent, e.g., $(La/Sm)_N$ and $(Ce/Yb)_N$ higher than 1, while their H_2O/Ce ratios are always lower than ~430 (Figs. 5a and 5b). As shown in Fig. 4b, the 55°E samples share the $H_2O_{(8)}$ vs. $(Ce/Yb)_N$ trends defined by other H_2O-rich oceanic ridges, but the 48-52°E samples have considerably lower $(Ce/Yb)_N$ ratios at a given $H_2O_{(8)}$, which suggest their mantle source is more depleted in incompatible elements. In addition, compared to glasses from the Arctic and 33~40°N MAR (Azores Platform basalts), which prior to this study had the highest H_2O/Ce among MORB, the 48°E to 52°E samples show a narrow range of $(La/Sm)_N$ near ~0.5 (Fig. 5a) and span a comparable range of Yb (and other incompatible element) with Arctic and Azores Platform basalts (Supplementary Fig. 7). Their low $(La/Sm)_N$ could not be formed simply by a larger extent of partial melting from a similar source, which would decrease the Yb content at the same time. Yang et al. (2017) suggested that the low $(La/Sm)_N$ found in SWIR MORB can be attributed to a contribution of the Crozet plume mantle, modified by prior melt extraction on the journey to the ridge. However, this scenario cannot be used to explain the observed high H_2O/Ce ratios. Due to that the partition coefficient of H_2O between garnet lherzolite and melt is slightly lower than that of Ce (Hauri et al., 2006), previous melt extraction of a hydrous plume mantle would decrease the H_2O/Ce ratio of the residual mantle (Hauri et al., 2006). In this regard, to explain our data, the H_2O/Ce ratio of the Crozet plume mantle would have to be >600 before melt extraction. Although mantle sources with H_2O/Ce ratios >3000 have been inferred for komatiites and picrites in some continental LIPs (Liu et al., 2017; Sobolev et al., 2016), the global Phanero-

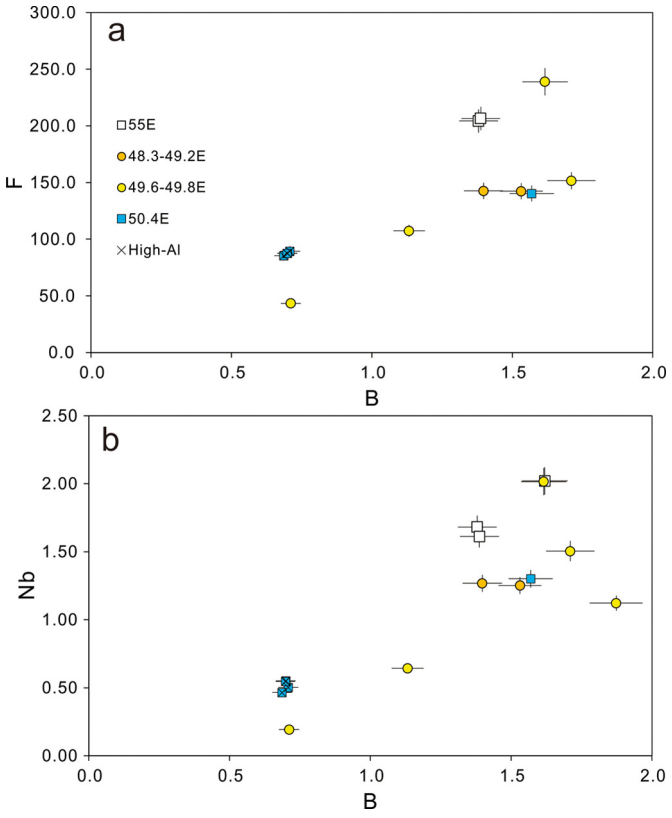

Fig. 6. The comparisons of B with F and Nb for the SWIR samples. All the data are included in the supplementary tables. Error bars represent uncertainty of 5%.

zoic OIBs and the oceanic plateaus never show H_2O/Ce ratios such high (Dixon and Clague, 2001; Kendrick et al., 2017, 2014; Wallace, 2002; Workman et al., 2004, 2006).

The alternative explanation for the water enrichment in MORB is the delivery of a mantle plume-sourced, volatile-rich low-degree melt through highly channelized flow towards the ridge (Gibson and Richards, 2018). However, two observations argue against this possibility in our case. First, the $H_2O_{(8)}$ vs. $(Ce/Yb)_N$ trend in Fig. 5b for the 48-52°E samples is considerably steeper than that of all other mid-ocean ridge-plume interaction pairs, which span a large range in spreading rates, mantle plume temperature and geochemical end-members. This discrepancy could not be explained by a larger degree of partial melting for the plume-derived melts in channelized flow, which would decrease the water content and $(Ce/Yb)_N$ simultaneously. Second, the most H_2O-rich MORBs show the tendency to occur near where large volcanic lineaments radiating from mantle plume stems intersect the ridge axis (Gibson and Richards, 2018), which is not observed in our case. On the other hand, recently published Sr-Nd-Pb isotope compositions for more abundant SWIR MORBs argue against contributions from both the western and eastern Crozet hotspot mantle (Wang et al., 2020; Yu and Dick, 2020). These considerations allow us to conclude that the high H_2O/Ce ratios, and high water contents of SWIR basalts are unlikely to be related to the interaction with the Crozet plume.

The water content of the oceanic crust would also be elevated in the cold regions along MORs, which are known as "cold spots" (e.g., the ridge close to a large-scale fracture zone) (Ligi et al., 2005; Robinson et al., 2001). The water enrichment in these ridges is considered to result from low degrees of melting occurring mostly within the "wet melting" depth interval below the ridge in the garnet stability field, with minor dilution from shallower melts (Ligi et al., 2005; Robinson et al., 2001). As shown in Fig. 8, these "cold spot" basalts (Atlantic ridge at 0° and 35°N) show considerably high $(Sm/Yb)_N$ ratio. In this figure, these samples are bracketed by the partial melts of a N-DMM mantle (Workman and Hart, 2005) with 200 ppm H_2O (the upper limit for the DMM) melted at spinel stability field and garnet stability field, respectively. Clearly, the mixing of these two kinds of melt could not explain most of the 48-52°E samples, which show $H_2O_{(8)}$ higher than 0.3 with $(Sm/Yb)_N$ lower than 1.1 (Fig. 8). In addition, the water contents are maximal in the central part of the SWIR segment (Fig. 8), which is far from the cold zone near the transformed fracture zone, the typical locus of "cold spots" (Ligi et al., 2005). Thus, we conclude that the "cold spots" mechanism is an unsatisfactory explanation for the SWIR data.

The H_2O/Ce ratios of the samples from 48°E to 52°E are at the lower end of the range of arc or back-arc lavas (Cooper et al., 2012) and significantly higher than the ratios in global OIBs and MORBs with affinities to different mantle end members (Dixon et al., 2002, 2017; Kendrick et al., 2017; Michael, 1995; Wallace, 2002; Workman et al., 2004). The high H_2O/Ce end member has heavy hydrogen isotope ratios ($\delta D > -40‰$), and radiogenic $^{87}Sr/^{86}Sr$ (>0.703) ratios (Fig. 5c, d). In addition, the calculated water contents in the mantle source and δD are negatively correlated with Ce/Pb ratios (Supplementary Fig. 5). These features are consistent with the characteristics of a mantle wedge that has been infiltrated by fluids derived from a subducting slab (Shaw et al., 2008) (Fig. 4c). The presence of mantle wedge segments that have experienced melt extraction related to ancient subduction events has been suggested for the SWIR (53°E, Fig. 1, 2) and Mid-Atlantic Ridges (Gao et al., 2016; Urann et al., 2020). Thus, the coupled high H_2O/Ce and depleted incompatible trace element signatures (e.g., low $(La/Sm)_N$, $(Ce/Yb)_N$) could be a contribution from an arc mantle residue after an ancient partial melting event. To test this possibility, we performed a calculation to model the observed H_2O/Ce ratios and trace element and isotope compositions (see Supplementary materials, Supplementary Table 7). The mixing between a partial melt derived from N-DMM (normal depleted MORB mantle, defined by Workman and Hart (2005)) and a partial melt derived from an arc mantle residuum with a chemical composition of the present Mariana sub-arc mantle after melt extraction, is shown in Figs. 5c and 5d and Fig. 7. This mixing can explain the relations between H_2O, trace elements and Sr-H isotopes of our samples, and also provide potential explanations to our B and $\delta^{11}B$ data (Fig. 7). Especially, our modeling also demonstrates that this mixing does not necessarily propagate to a positive Pb anomaly (Fig. 9). It deserves to note although the arc magma usually has high Ba/Nb, low Ce/Pb and Sr/Nd ratios, but not necessarily the arc mantle residual does. These elemental ratios of the mantle residue depend on the elemental partitioning coefficients. The Ba/Nb ratio of one wedge residual after melt extraction could span a large range from less one to 17 (based on a subset of arc magma data from the GEOROCK database), while the ratios for the equilibrium arc magma could be as high as ~200. Such large change is due to the large difference in element partition coefficient (0.00012 for Ba vs. 0.0034 for Nb, data from Workman and Hart, 2005; Kelley et al., 2008). This process is also true for Sr/Nd and Ce/Pb ratios. In summary, we conclude that the residue of a hydrous partial melting in mantle wedge after the genesis of arc magmatism could best explain the water rich reservoir responsible for the high H_2O/Ce ratio for the SWIR basalts.

4.4. Possible role of water in the enhancement of magmatic activity

The production of the super-thick oceanic crust at 50.6°E has been explained by several models, including focused melt flow (Cannat et al., 2008; Li et al., 2015) or interaction with the Crozet hotspot (Sauter et al., 2009; Yang et al., 2017). Yu and Dick (2020) attributed this melting anomaly to the upwelling of the shallow upper mantle caused by the plate reorganization. They also sug-

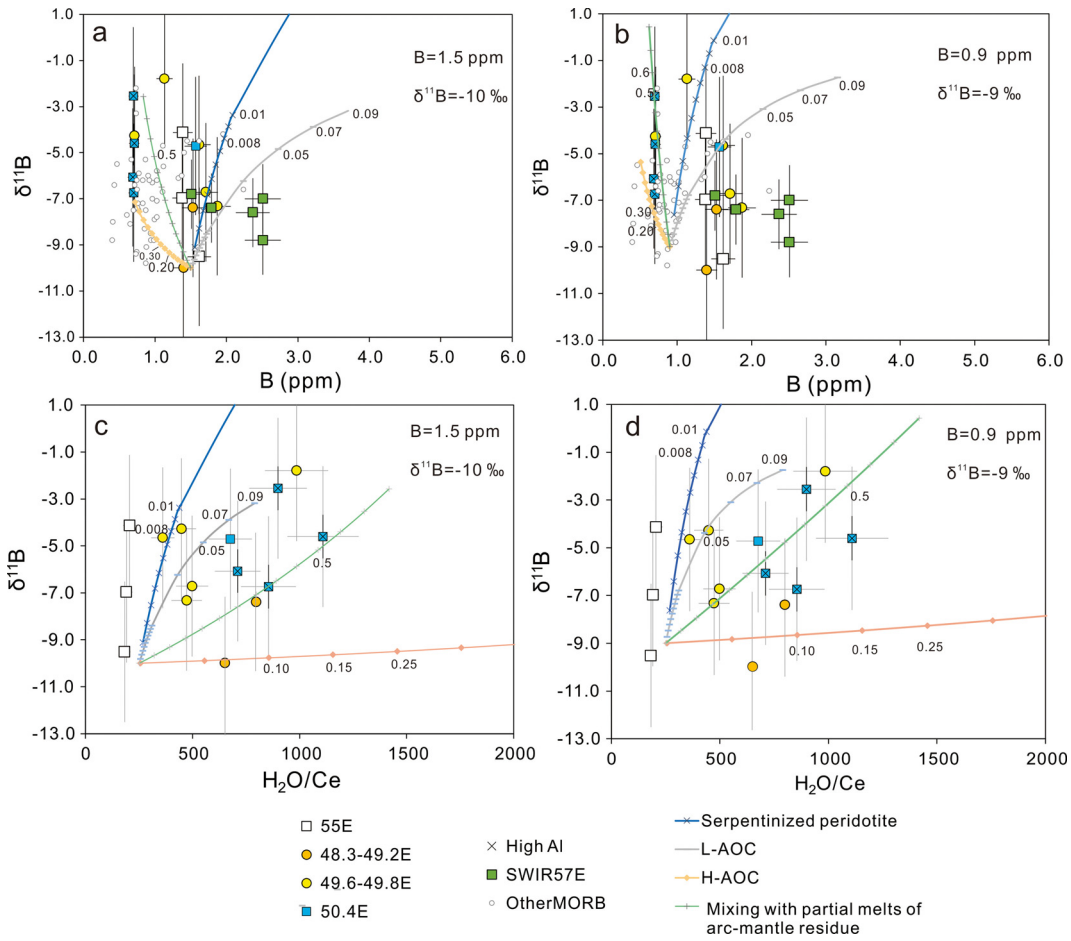

Fig. 7. The comparison of δ^{11}B with B content and H_2O/Ce. The data for SWIR 57 °E and other MORBs (EPR, MAR, Galapagos) are from Marschall et al. (2017). The curves show the modeling of the assimilations between the assumed fresh sample with different hydrous components (L-AOC, low-temperature altered oceanic crust; H-AOC, high-temperature altered oceanic crust; Serpentinized peridotite). B content and δ^{11}B for L-AOC, H-AOC and Serpentitnized peridotite are: 26 ppm and 0.8‰, 0.3 ppm and 0.5‰, 60 ppm and 13‰ respectively (Marschall et al., 2017; Boschi et al., 2013). The composition of the partial melts of the arc-mantle residue was calculated by assuming that this residue has 600 ppm water, 0.035 ppm B with δ^{11}B of 10‰ and H_2O/Ce ratio of ~2500. The partial melting degree of this mantle residue is assumed to be 4%. For a and c, the initial compositions of the fresh glass are B content of 1.5 ppm, and δ^{11}B of -10‰ (similar with the lower limit in our SWIR data), while for b and d the initial values are B content of 0.9 ppm and δ^{11}B of -9‰. The numbers near the curves show the percentage of the assimilated components. See the modeling data for these curves in Supplementary Table 8.

gested that increase of melt influx followed a major change in the source composition drawn into the melting column, although what kind of this change was not demonstrated. As shown in Fig. 3, minima in the ridge water depth are mirrored by maxima in the H_2O content and H_2O/Ce ratio, even if the high-Al group samples are not considered. These observations suggest that the magmatic activity along the ridge was also associated with heterogeneities of the mantle hydration state, not the simple focused melt flow to the center of the ridge segment occurred. It is well known that the water enrichment in the upwelling asthenosphere beneath an ocean ridge could deepen the solidus depth to the garnet stability field (>70 km) even at a normal ridge adiabatic thermal gradient and increase the total melt production and crustal thickness while decreasing the mean extent of melting (Asimow and Langmuir, 2003; Hirschmann, 2006; Katz et al., 2003). One striking geochemical observation in the MORBs associated with a H_2O-rich source is the highly fractionated $(Sm/Yb)_N$ ratio of up to ~3.52±1.42 (Asimow and Langmuir, 2003; Ligi et al., 2005; Robinson et al., 2001) (Fig. 8). Although mixing with spinel-stability-field melts would potentially dilute this signature, it is more difficult for this mechanism to affect all basalts along the entire ridge segment. The unfractionated $(Sm/Yb)_N$ for the 48-52°E basalts (0.99±0.20, 2SD) thus suggests that the partial melting regime beneath the ocean ridge would mainly occur at a shallow depth of <70 km. One explanation for the association of high water contents with non-fractionated heavy rare earth element patterns is that the water reservoir resides in the mantle shallower than the garnet stability field, which makes the initial melting shallow. This can be reconciled with our previous conclusion that the water-rich reservoir for the 48-52°E is an ancient wedge mantle residuum, which may be buoyant in the upper mantle for a long time (Urann et al., 2020; Gao et al., 2016). As suggested by Yu and Dick (2020), the source of the melting anomaly at 50.6°E could be the delaminated or sheared off ancient continental lithospheric fragments that include old depleted supra subduction zone mantle with entrained subducted Archean and Neoproterozoic sediments, and old Mozambique Ocean crust, and numerous Neoproterozoic arc and back-arc lithospheric fragments including metasomatized older Archean lithosphere. They also suggested that those isotopically enriched components foundered in the asthenosphere during the Gondwanan breakup (Yu and Dick, 2020), and dispersively "contanminated" the upper mantle. This would explain why such kind of mantle component is not commonly seen along other ridges.

5. Conclusions

The origin of the water in the upper mantle continues to be a topic of debate. Suggested origins include residues of partial melt-

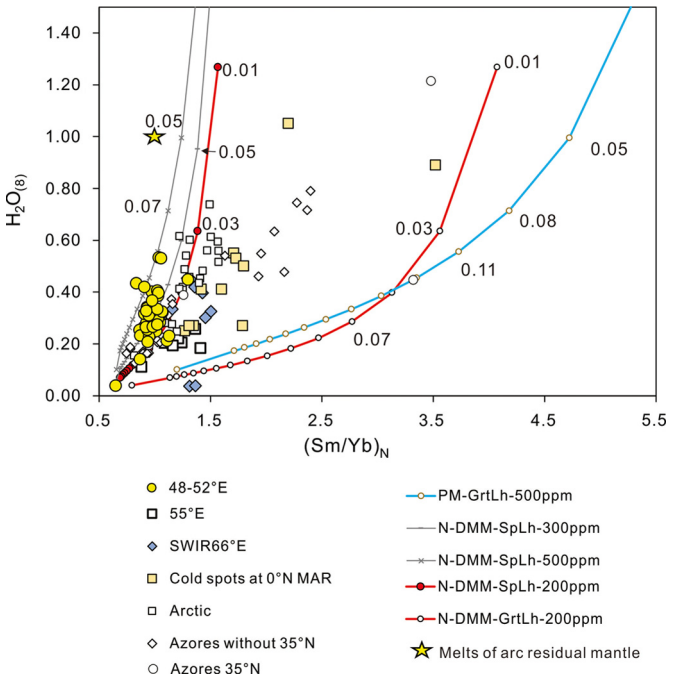

Fig. 8. The comparison of $H_2O_{(8)}$ with $(Sm/Yb)_N$ for the SWIR glasses in this study. The red lines show the modeled variation of water content and $(Sm/Yb)_N$ for the partial melts of the normal depleted MORB source (N-DMM) with initial water content of 200 ppm. The accumulated fractional melting mode is applied. The gray lines demonstrate the modeled composition for the partial melts of N-DMM with 300 and 500 ppm water. SpLh represents spinel lherzolite, GrtLh represent garnet lherzolite. The blue line shows the modeled melt composition for a mantle with primitive mantle-like Sm and Yb content, and 500 ppm water. The numbers along the lines are the partial melting degree in the calculation. The Sm and Yb concentration of N-DMM are from Workman and Hart (2005), and that of primitive mantle are from McDonough and Sun (1995). The partition coefficients of Sm and Yb between spinel lherzolite and basaltic melt are from Workman and Hart (2005), and that between garnet lherzolite and basaltic melt are from Stracke and Bourdon (2009). The data are from this study, Dixon et al. (2017), Ligi et al. (2005), and Robinson et al. (2001), and the references therein.

ing of H_2O-rich material advected through 410 km discontinuity (Bercovici and Karato, 2003), of hydrous melting in mantle wedges (Hirth and Kohlstedt, 2003), and of plumes beneath oceanic islands (Phipps Morgan and Morgan, 1999). While it is beyond the scope of this work to model how the wedge mantle would escape and react with the ambient upper mantle, our results show that in the ultra-slow spreading SWIR, the basalts could have considerably higher H_2O/Ce ratios than the global MORBs, and the high H_2O/Ce ratios are associated with heavy δD and low Ce/Pb ratios. The SWIR water-rich glasses show considerably low La/Sm, Ce/Yb and Sm/Yb ratios, which are in big contrast to the water-enrichment glasses from other ridge basalts effected by the mantle plume nearby. We conclude that these results could be best explained by the involvement of the arc-mantle wedge residue after early melt extraction in the ridge mantle (Fig. 10). This study provides evidence for recycling of water in the mantle wedge residua to the sub-ocean asthenosphere without a need of interaction with a mantle plume. The possible role of this shallow cycling should be seriously considered in studies of global water recycling between the Earth's surface and deep interior and the origin of water in the upper asthenosphere.

CRediT authorship contribution statement

Jia Liu: Conceptualization, Methodology, Formal analysis, Funding acquisition, Writing-Original

Chunhui Tao: Conceptualization, Writing - Review & Editing, Funding acquisition

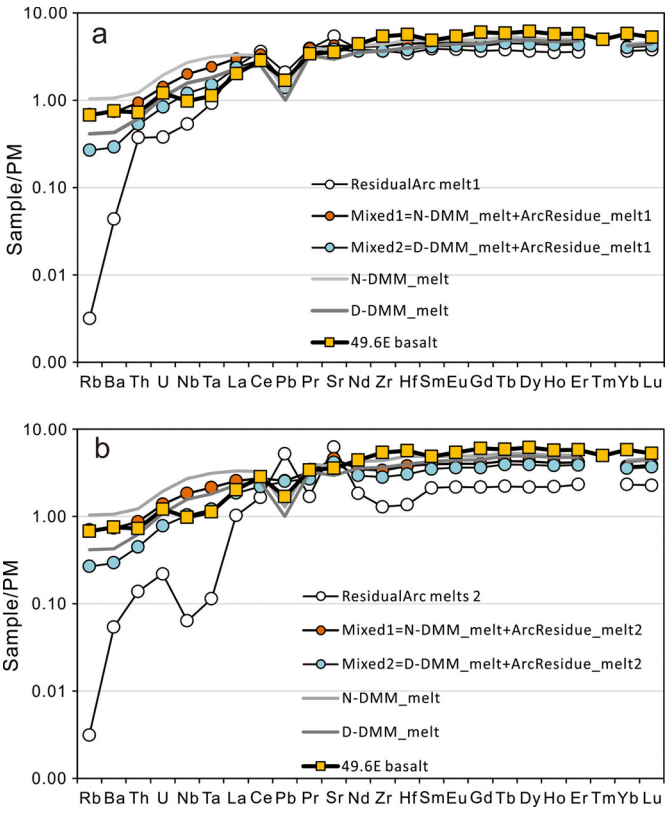

Fig. 9. The trace elemental pattern of the modeled partial melts derived from the arc-mantle residuum and its mixture with DMM-derived partial melts. **a**, the case arc mantle residual in equilibrium with Mariana back-arc basalt. N-DMM_melt and D-DMM_melt are the calculated partial melt of normal and depleted DMM (N-DMM, D-DMM, Workman and Hart, 2005) respectively, with partial melting degree assumed to be 8% in the model. The arc residual mantle is equilibrium with the Mariana back-arc basalt, with partial melting degree of 4%. Partition coefficients are from Workman and Hart (2005). **b**, the case arc mantle residual in equilibrium with Mariana arc front basalt. The composition of other components in the mode is same with that in **a**. The primitive mantle composition used for the normalization is from McDonough and Sun (1995). The composition, partition coefficients and modeled data are listed in Supplementary Table 7.

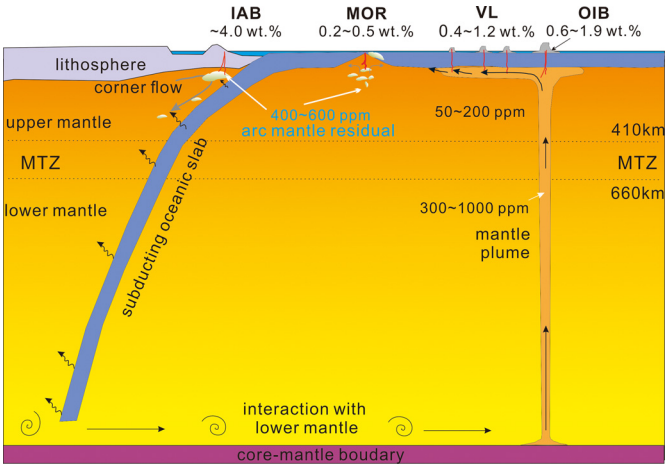

Fig. 10. Cartoon showing the mechanisms that enhance the water content in the mid-ocean ridge mantle. The subduction of altered oceanic lithosphere, recycling of its hydrous derivatives by the mantle plume, and the ridge-plume interaction through either solid mantle flow or low degree partial melt channelized flow, provide the traditional approach for the water enrichment in many ridges (the black arrows). The arc mantle residual dragged down by the subducting plate, equilibrium with the hydrous arc basalts, provides the alternative candidate to supply water in the MOR. IAB, island arc basalts; VL, volcanic lineament, which is usually observed between the hotspot and the MOR interacted with it.

Jianping Zhou: Methodology,
Kenji Shimizu: Methodology, Writing - Review & Editing, Funding acquisition
Wei Li: Visualization
Jin Liang: Visualization
Shili Liao: Visualization
Takeshi Kuritani: Methodology, Writing - Review & Editing
Etienne Deloule: Methodology
Takayuki Ushikubo: Methodology
Mitsuhiro Nakagawa: Methodology
Weifang Yang: Resources
Guoyin Zhang: Resources, Visualization
Yunlong Liu: Visualization
Chuanwei Zhu: Visualization
Hao Sun: Methodology
Jingjun Zhou: Methodology, Visualization

Declaration of competing interest

The authors declare that they have no known competing financial interests or personal relationships that could have appeared to influence the work reported in this paper.

Acknowledgements

This work was supported by the National Key R&D Program of China (2018YFC0309902, 2018YFC0309901), the National Natural Science Foundation of China (42022019), the COMRA Major Project (DY135-S1-01-03, DY135-S1-01-01), and the JSPS KAKENHI (15H03751, 18H01320) to K.S. We thank Jihao Zhu, Suwen Qiu, Can Rao, Yantao Hao, and Ting Liang for their assistance in EPMA and LA-ICP-MS analysis. The Dayangyihao and Xiangyanghong 10 R/V and the COMA were thanked for their support to the conduction of cruises. Ingrin Jannick, Eero Hanski and Marc Hirschmann are thanked for the comments and suggestions to the early version of the manuscript. Liu thanks Yang Yang and Xing Yu for the fruitful discussions. We appreciate the thorough comments and suggestions from Jacqueline E. Dixon and the anonymous reviewer, and the handling by the editor Rosemary Hickey-Vargas.

Appendix A. Supplementary material

Supplementary material related to this article can be found online at https://doi.org/10.1016/j.epsl.2022.117455.

References

Asimow, P.D., Langmuir, C.H., 2003. The importance of water to oceanic mantle melting regimes. Nature 7, 815–820.
Bercovici, D., Karato, S.I., 2003. Whole-mantle convection and the transition-zone water filter. Nature 425, 39–44. https://doi.org/10.1038/nature01918.
Bonatti, E., 1990. Not so hot "hot spots" in the oceanic mantle. Nature 137, 107–111.
Boschi, C., Bonatti, E., Ligi, M., Brunelli, D., Cipriani, A., Dallai, L., D'Orazio, M., Früh-Green, G.L., Tonarini, S., Barnes, J.D., Bedini, R.M., 2013. Serpentinization of mantle peridotites along an uplifted lithospheric section, mid Atlantic ridge at 11° N. Lithos 178, 3–23. https://doi.org/10.1016/j.lithos.2013.06.003.
Bouvier, A.S., Métrich, N., Deloule, E., 2008. Slab-derived fluids in the magma sources of St. Vincent (Lesser Antilles Arc): volatile and light element imprints. J. Petrol. 49, 1427–1448.
Cai, Y., Yang, A.Y., Goldstein, S.L., Langmuir, C.H., Michael, P.J., Cochran, J.R., Bolge, L., 2021. Multi-stage melting of enriched mantle components along the eastern Gakkel Ridge. Chem. Geol. 586, 120594.
Cannat, M., Sauter, D., Bezos, A., Meyzen, C., Humler, E., Rigoleur, M. Le, 2008. Spreading rate, spreading obliquity, and melt supply at the ultraslow spreading Southwest Indian Ridge. Geochem. Geophys. Geosyst. 9, Q04002. https://doi.org/10.1029/2007GC001676.
Cooper, L.B., Ruscitto, D.M., Plank, T., Wallace, P.J., Syracuse, E.M., Manning, C.E., 2012. Global variations in H2O/Ce:1. Slab surface temperatures beneath volcanic arcs. Geochem. Geophys. Geosyst. 13, Q03024. https://doi.org/10.1029/2011GC003902.
Danyushevsky, L.V., Eggins, S.M., Falloon, T.J., Christie, D.M., 2000. H2O abundance in depleted to moderately enriched mid-ocean ridge magmas; Part I: incompatible behaviour, implications for mantle storage, and origin of regional variations. J. Petrol. 41, 1329–1364. https://doi.org/10.1093/petrology/41.8.1329.
Dixon, J.E., Bindemean, I.N., Kingsley, R.H., Simons, K.K., Le Roux, P.j., Hajewski, T.R., Swart, P., Langmuir, C.H., Ryan, L.G., Walowski, K.J., Wada, I., Wallace, P., 2017. Light stable isotopic compositions of enriched mantle sources: resolving the dehyration paradox. Geochem. Geophys. Geosyst. 18, 1–39.
Dixon, J.E., Clague, D.A., 2001. Volatiles in basaltic glasses from Loihi seamount, Hawaii: evidence for a relatively dry plume component. J. Petrol. 42, 627–654.
Dixon, J.E., Leist, L., Langmuir, C.H., Schilling, J., 2002. Recycled dehydrated lithosphere observed in plume-influenced mid-ocean-ridge basalt. Nature 420, 385–389. https://doi.org/10.1038/nature01215.
Dixon, J.E., Stolper, E.M., Holloway, J., 1995. An experimental study of water and carbon dioxide solubilities in mid-ocean ridge basaltic liquids. Part I: calibration and solubility models. J. Petrol. 36, 1607–1631.
Gale, A., Dalton, C.A., Langmuir, C.H., 2013. The mean composition of ocean ridge basalts. Geochem. Geophys. Geosyst. 14, 489–518. https://doi.org/10.1029/2012GC004334.
Gao, C., Dick, H.J.B., Liu, Y., Zhou, H., 2016. Melt extraction and mantle source at a Southwest Indian Ridge Dragon Bone amagmatic segment on the Marion Rise. Lithos 246–247, 48–60. https://doi.org/10.1016/j.lithos.2015.12.007.
Gibson, S.A., Richards, M.A., 2018. Delivery of deep-sourced, volatile-rich plume material to the global ridge system. Earth Planet. Sci. Lett. 499, 205–218.
Hallis, L.J., Huss, G.R., Nagashima, K., Taylor, G.J., Halldórsson, S.A., Hilton, D.R., Mottl, M.J., Meech, K.J., 2015. Evidence for primordial water in Earth's deep mantle. Science 350, 795–797.
Hartley, M.E., Neave, D.A., Maclennan, J., Edmonds, M., Thordarson, T., 2015. Diffusive over-hydration of olivine-hosted melt inclusions. Earth Planet. Sci. Lett. 425, 168–178. https://doi.org/10.1016/j.epsl.2015.06.008.
Hauri, E.H., Gaetani, G.A., Green, T.H., 2006. Partitioning of water during melting of the Earth's upper mantle at H2O-undersaturated conditions. Earth Planet. Sci. Lett. 248, 715–734. https://doi.org/10.1016/j.epsl.2006.06.014.
Hirschmann, M.M., 2006. Water, melting, and the deep Earth H_2O cycle. Annu. Rev. Earth Planet. Sci. 34, 629–653.
Hirth, G., Kohlstedt, D., 2003. Rheology of the upper mantle and the mantle wedge: a view from the experimentalists upper mantle. In: Geophys. Monogr. Geophys. Union, vol. 138, pp. 83–106.
Jamtveit, B., Brooker, R., Brooks, K., Larsen, L.M., Pedersen, T., 2001. The water content of olivines from the North Atlantic volcanic province. Earth Planet. Sci. Lett. 186, 401–415. https://doi.org/10.1016/S0012-821X(01)00256-4.
Katz, R.F., Spiegelman, M., Langmuir, C.H., 2003. A new parameterization of hydrous mantle melting. Geochem. Geophys. Geosyst. 4, 1073.
Kelley, K.A., Plank, T., Grove, T.L., Stolper, E.M., Newman, S., Hauri, E.H., 2006. Mantle melting as a function of water content beneath back-arc basins. J. Geophys. Res. 111. https://doi.org/10.1029/2005JB003732.
Kendrick, M., Hémond, C., Kamenetsky, V., Danyushevsky, L., Devey, C.W., Rodemann, T., Jackson, M.G., Perfit, M., 2017. Seawater cycled throughout Earth's mantle in partially serpentinized lithosphere. Nat. Geosci. 10, 222–228. https://doi.org/10.1038/NGEO2902.
Kendrick, M.A., Jackson, M.G., Kent, A.J.R., Hauri, E.H., Wallace, P.J., Woodhead, J., 2014. Contrasting behaviours of CO_2, S, H_2O and halogens (F, Cl, Br, and I) in enriched-mantle melts from Pitcairn and Society seamounts. Chem. Geol. 370, 69–81.
Li, J., Jian, H., Chen, Y.J., Singh, S.C., Ruan, A., Qiu, X., Zhao, M., Wang, X., Niu, X., Ni, J., Zhang, J., 2015. Seismic observation of an extremely magmatic accretion at the ultraslow spreading Southwest Indian Ridge. Geophys. Res. Lett. 42, 2656–2663. https://doi.org/10.1002/2014GL062521.
Ligi, M., Bonatti, E., Cipriani, A., Ottolini, L., 2005. Water-rich basalts at mid-ocean-ridge cold spots. Nature 434, 66–69. https://doi.org/10.1038/nature03264.
Liu, J., Xia, Q.-K., Kuritani, T., Hanski, E., Yu, H.-R., 2017. Mantle hydration and the role of water in the generation of large igneous provinces. Nat. Commun. 8, 1824. https://doi.org/10.1038/s41467-017-01940-3.
Liu, Y., Hu, Z., Gao, S., Günther, D., Xu, J., Gao, C., Chen, H., 2008. In situ analysis of major and trace elements of anhydrous minerals by LA-ICP-MS without applying an internal standard. Chem. Geol. 257, 34–43. https://doi.org/10.1016/j.chemgeo.2008.08.004.
Marschall, H.R., Wanless, V.D., Shimizu, N., Von Strandmann, P.A.P., Elliott, T., Monteleone, B.D., 2017. The boron and lithium isotopic composition of mid-ocean ridge basalts and the mantle. Geochim. Cosmochim. Acta 207, 102–138.
McDonough, W.F., Sun, S.-S., 1995. The composition of the Earth. Chem. Geol. 120, 223–253.
Michael, P., 1995. Regionally distinctive sources of depleted MORB: evidence from trace elements and H_2O. Earth Planet. Sci. Lett. 131, 301–320.
Phipps Morgan, J., Morgan, W.J., 1999. Two-stage melting and the geochemical evolution of the mantle: a recipe for mantle plum-pudding. Earth Planet. Sci. Lett. 170, 215–239. https://doi.org/10.1016/S0012-821X(99)00114-4.
Pin, C., Briot, D., Bassin, C., Poitrasson, F., 1994. Concomitant separation of strontium and samarium-neodymium for isotopic analysis in silicate samples, based on specific extraction chromatography. Anal. Chim. Acta 298 (2), 209–217.

Pin, C., Zalduegui, J.S., 1997. Sequential separation of light rare-Earth elements, thorium and uranium by miniaturized extraction chromatography: application to isotopic analyses of silicate rocks. Anal. Chim. Acta 339, 79–89.

Robinson, C.J.Y., Bickle, M.J., Minshull, T.A., White, R.S., 2001. Low degree melting under the Southwest Indian Ridge: the roles of mantle temperature, conductive cooling and wet melting. Earth Planet. Sci. Lett. 188, 383–398.

Saal, A.E., Hauri, E.H., Langmuir, C.H., Perfit, M.R., 2002. Vapour undersaturation in primitive mid-ocean-ridge basalt and the volatile content of Earth's upper mantle. Nature 419, 451–455. https://doi.org/10.1038/nature01073.

Salters, V.J., Stracke, A., 2004. Composition of the depleted mantle. Geochem. Geophys. Geosyst. 5 (5), Q05B07. https://doi.org/10.1029/2003GC000597.

Sauter, D., Cannat, M., Meyzen, C., Bezos, A., Patriat, P., Humler, E., Debayle, E., 2009. Propagation of a melting anomaly along the ultraslow Southwest Indian Ridge between 46° E and 52° 20 E: interaction with the Crozet hotspot? Geophys. J. Int. 179, 687–699. https://doi.org/10.1111/j.1365-246X.2009.04308.x.

Shaw, A.M., Hauri, E.H., Fischer, T.P., Hilton, D.R., Kelley, K.A., 2008. Hydrogen isotopes in Mariana arc melt inclusions: implications for subduction dehydration and the deep-Earth water cycle. Earth Planet. Sci. Lett. 275, 138–145. https://doi.org/10.1016/j.epsl.2008.08.015.

Shimizu, K., Matsu, F., Agency, E., Ueno, Y., 2019. In situ analyses of hydrogen and sulfur isotope ratios in basaltic glass using SIMS. Geochem. J. 53, 195–207. https://doi.org/10.2343/geochemj.2.0559.

Shimizu, K., Ushikubo, T., Hamada, M., Itoh, S., Higashi, Y., Takahashi, E., Ito, M., 2017. H_2O, CO_2, F, S, Cl, and P_2O_5 analyses of silicate glasses using SIMS: Report of volatile standard glasses. Geochem. J. 51, 299–313. https://doi.org/10.2343/geochemj.2.0470.

Simons, K., Dixon, J., Schilling, J.-G., Kingsley, R., Poreda, R., 2002. Volatiles in basaltic glasses from the Easter-Salas y Gomez Seamount Chain and Easter Microplate: implications for geochemical cycling of volatile elements. Geochem. Geophys. Geosyst. 3. https://doi.org/10.1029/2001GC000173.

Sobolev, A.V., Asafov, E.V., Gurenko, A.A., Arndt, N.T., Batanova, V.G., Portnyagin, M.V., Garbe-Schönberg, D., Krasheninnikov, S.P., 2016. Komatiites reveal a hydrous Archaean deep-mantle reservoir. Nature 531, 628–632. https://doi.org/10.1038/nature17152.

Stracke, A., Bourdon, B., 2009. The importance of melt extraction for tracing mantle heterogeneity. Geochim. Cosmochim. Acta 73, 218–238. https://doi.org/10.1016/j.gca.2008.10.015.

Sun, S.S., McDonough, W.F., 1989. Chemical and isotopic systematics of oceanic basalts: implications for mantle composition and processes. Geol. Soc. Spec. Publ. 42, 313–345. https://doi.org/10.1144/GSL.SP.1989.042.01.19.

Urann, B.M., Dick, H.J.B., Casey, J.F., 2020. Recycled arc mantle recovered from the mid- Atlantic ridge. Nat. Commun. 11, 3887.

Voyer, M.Le, Cottrell, E., Kelley, K.A., Brounce, M., Hauri, E.H., 2014. The effect of primary versus secondary processes on the volatile content of MORB glasses: an example from the equatorial mid Atlantic ridge (5°N–3°S). J. Geophys. Res., Solid Earth 120, 125–144. https://doi.org/10.1002/2014JB011160.

Wallace, P.J., 2002. Volatiles in submarine basaltic glasses from the Northern Kerguelen plateau (ODP site 1140): implications for source region compositions, magmatic processes, and plateau subsidence. J. Petrol. 43, 1311–1326.

Wang, J., Zhou, H., Salters, V.J.M., Dick, H.J.B., Standish, J.J., Wang, C., 2020. Trace element and isotopic evidence for recycled lithosphere from basalts from 48 to 53°E, Southwest Indian Ridge. J. Petrol. 61, egaa068. https://doi.org/10.1093/petrology/egaa068.

Wang, W., Kelley, K.A., Li, Z., Chu, F., Dong, Y., Chen, L., Dong, Y., Li, J., 2021. Volatile element evidence of local MORB mantle heterogeneity beneath the Southwest Indian Ridge, 48°–51°E. Geochem. Geophys. Geosyst. 22, e2021GC009647. https://doi.org/10.1029/2021GC009647.

Workman, R.K., Hart, S.R., 2005. Major and trace element composition of the depleted MORB mantle (DMM). Earth Planet. Sci. Lett. 231, 53–72. https://doi.org/10.1016/j.epsl.2004.12.005.

Workman, R.K., Hart, S.R., Jackson, M., Regelous, M., Farley, K.A., Blusztajn, J., Kurz, M., Staudigel, H., 2004. Recycled metasomatized lithosphere as the origin of the enriched mantle II (EM2) end-member: evidence from the samoan volcanic chain. Geochem. Geophys. Geosyst. 5, Q04008. https://doi.org/10.1029/2003GC000623.

Workman, R.K., Hauri, E., Hart, S.R., Wang, J., Blusztajn, J., 2006. Volatile and trace elements in basaltic glasses from Samoa: implications for water distribution in the mantle. Earth Planet. Sci. Lett. 241, 932–951. https://doi.org/10.1016/j.epsl.2005.10.028.

Yang, A.Y., Zhao, T.P., Zhou, M.F., Deng, X.G., 2017. Isotopically enriched n-MORB: a new signature of off-axis plume-ridge interaction— a case study at 50°280E, Southwest Indian Ridge. J. Geophys. Res., Solid Earth 122, 191–213. https://doi.org/10.1002/2016JB013284.

Yang, A.Y., Langmuir, C.H., Cai, Y., Michael, P., Goldstein, S.L., Chen, Z., 2021. A subduction influence on ocean ridge basalts outside the Pacific subduction shield. Nat. Commun. 12, 4757.

Yu, X., Dick, H.J.B., 2020. Plate-driven micro-hotspots and the evolution of the Dragon Flag melting anomaly, Southwest Indian Ridge. Earth Planet. Sci. Lett. 531. https://doi.org/10.1016/j.epsl.2019.116002.

Zhang, Y., Stolper, E.M., 1991. Water diffusion in a basaltic melt. Nature 351, 306–309.

Zhou, H., Dick, H.J.B., 2013. Thin crust as evidence for depleted mantle supporting the Marion Rise. Nature 494, 195–200. https://doi.org/10.1038/nature11842.